Quantum signatures of an integrable system with a chaotic scattering map

1995 J. Phys. A: Math. Gen. 28 1507

(http://iopscience.iop.org/0305-4470/28/6/008)

J. Phys. A: Math. Gen. 28 (1995) 1507–1519. Printed in the UK

Quantum signatures of an integrable system with a chaotic scattering map

C Jung and T H Seligman

University of Mexico (UNAM), Instituto de Física, Laboratorio de Cuernavaca, 62191 Cuernavaca, Mexico

Received 16 August 1994

Abstract. A rather simple completely integrable Hamiltonian with a chaotic classical scattering map is analysed in quantum mechanics. After the analytical computation of the S-matrix we investigate numerically the distribution of scattering phases, giving the nearest-neighbour distribution, the number variance and the Fourier transform of the spectrum. We find fair agreement with the random matrix prediction for the circular orthogonal ensemble (COE) as appropriate for the time-reversal invariant system with a chaotic scattering map. This example confirms that COE properties of the S-matrix do not necessarily indicate topological chaos in the flow generated by the classical Hamiltonian.

1. Introduction

The relation between classical chaos and random matrix fluctuations [1] in the corresponding quantum systems is based on three types of analysis. First and most common is the numerical analysis of simple quantum systems. Most of these analyses refer to energy spectra [2–9]. Some similar considerations exist for quasi-energies [10, 11] while work on the S-matrix is very limited [12]. The second type of analysis was introduced by Berry [13], who derived the Gaussian orthogonal ensemble [1] two-point function from the Selberg–Gutzwiller trace formula; this work was generalized by Blümel and Smilansky [14] to the quasi-energies and eigenphases of S-matrices. A general proof not limited to two-point functions was given in [15, 16], based on unitary representations of the structural invariance group of the chaotic scattering map.

When considering quantum signatures of chaotic scattering systems we could use two different concepts of classical chaos: on one hand the usual definition of toplogical chaos for Hamiltonian flows, and, on the other hand, the chaoticity of the classical scattering map which is the classical counterpart of the S-matrix. Unfortunately the two concepts are not equivalent, and the less common notion of a chaotic scattering map seems to be relevant in this context if we follow [14–16].

One of the authors (CJ) has given examples [17, 18] for situations where integrable Hamiltonians lead to chaotic scattering maps. In [19] the quantum properties of such systems were studied; yet these systems have the drawback that the 'free' Hamiltonian is complicated and possibly ambiguous. This is particularly disturbing as the definition of a chaotic scattering map depends sensitively on the interplay of the full Hamiltonian and the free Hamiltonian [17].

It thus seems of interest to study in quantum mechanics the simplest Hamiltonian

$$H = p_r^2/2 + (p_\phi^2 + \cos(\phi) + c)/2r^2 \tag{1}$$

0305-4470/95/061507+13$19.50

given in [18]. Here r, ϕ are polar coordinates in position space, p_r, p_ϕ are the conjugate momenta and c is a free constant. We shall find that the S-matrix can be obtained analytically as we may expect for an integrable system, yet the eigenphases display COE (circular orthogonal ensemble [1]) statistics as required for a quantum analogue of a chaotic scattering map. Thus we see that both aspects of chaos are relevant to the quantum scattering system.

In order to proceed let us start by giving a few definitions and relations to clarify the two relevant notions of scattering chaos.

Topological chaos may be defined as follows. In the open energy surface there exist unstable periodic orbits having transverse homoclinic and heteroclinic connections leading to topological chaos in the flow and to a Smale horseshoe in some appropriate Poincaré map. This, in turn, implies the existence of a chaotic saddle in the phase space having an infinity of unstable periodic orbits and an over countable number of localized non-periodic orbits. The invariant manifolds of the localized orbits reach into the asymptotic region causing singularities of the scattering functions (deflection function, time delay function etc) on a fractal subset of their domain.

The classical counterpart of the S-matrix is the classical iterated scattering map M which can be constructed as follows (see also [20–22]). M maps the set of all incoming scattering asymptotes into itself by the following construction. Given the initial asymptote A construct the full scattering trajectory starting with A, it ends in the outgoing asymptote B. Apply the time reversed free flow generated by H_0 on B in order to turn it back into an incoming asymptote C. Define $M(A) = C$.

For a system with two degrees of freedom M acts on a two-dimensional domain and a numerical investigation of M is done in the spirit of a Poincaré return map. Take a few initial points and iterate them numerically a large number of times by M. If the map M is integrable then all iterates of any initial point lie on one-dimensional lines. If the map is chaotic then the iterates of some initial points fill in densely a subset of higher dimension.

Whenever the Hamiltonian is completely integrable then the existence of horseshoes and of topological chaos in the flow is impossible. Surprisingly, the complete integrability of the Hamiltonian H does not necessarily imply the integrability of the classical scattering map or, equivalently, of the S-matrix. If K is a conserved quantity of H, i.e. $\{K, H\} = 0$, then K implies a conserved quantity J of S only if the asymptotic forward limit K_+ and the asymptotic backward limit K_- of K are equal among themselves, i.e. if

$$K_+ = K_-. \tag{2}$$

Here the asymptotic limits of K are defined classically as

$$K_\pm = \lim_{T \to \pm\infty} K \circ F(-T) \circ F_0(T) \tag{3}$$

where F and F_0 are the flow maps of the full Hamiltonian H and of the free asymptotic Hamiltonian H_0 respectively. Quantum mechanically the asymptotic limits of K are given by

$$K_\pm = \Omega_\pm^\dagger K \Omega_\pm \tag{4}$$

where $\Omega_\pm$ are the Moller operators. Integrability of H is transferred to M only if the conserved quantities of H fulfil the asymptotic condition (2). For details and proofs of all these statements see [17, 18].

2. The S-matrix

Let us consider the scattering of a mass point of mass $m = 1$ off a local potential in a two-dimensional position space. In polar coordinates (r, ϕ), the potential has the form

$$V(r, \phi) = f(\cos(\phi))/2r^2. \tag{5}$$

The function f has to be positive in order to avoid any problems with attractive singularities. The free asymptotic Hamiltonian is the kinetic energy

$$H_0 = p_r^2/2 + p_\phi^2/2r^2 \tag{6}$$

where p_r, p_ϕ are the momenta conjugate to (r, ϕ). It is obvious that the full Hamiltonian

$$H = H_0 + V \tag{7}$$

separates in polar coordinates and has the independent second conserved quantity

$$K = p_\phi^2 + f(\cos(\phi)). \tag{8}$$

Because of the homogeneity of the potential of degree -2 we not only have scaling but, for the S-matrix, there is, in fact, no energy dependence at all. We restrict all numerical computations to the single energy value $E = 0.5$. For a two-dimensional system the cross section contains the trivial over all energy factor $E^{-1/2}$.

There are no localized orbits and this prevents topological chaos in phase space. As a consequence each point in phase space belongs to a scattering trajectory having a proper incoming asymptote and a proper outgoing asymptote and there are no trajectories stuck in the interaction zone. Accordingly the classical scattering functions do not show any singularities.

The asymptotic forward and backward limit of p_ϕ is p_ϕ itself. Considering that in the distant future the position angle coincides with the momentum angle for any outoing asymptote, we find as forward limit of the position angle ϕ the momentum angle $\tan^{-1}(p_y/p_x)$. This leads to $p_x/|p|$ for the forward asymptotic limit of $\cos(\phi)$, where $|p|$ is the absolute value of the asymptotic momentum, i.e. $|p| = (2E)^{1/2}$. In the same way the backward limit of ϕ is $\tan^{-1}(p_y/p_x) + \pi$ because in the distant past the position angle is just opposite to the momentum angle for any incoming asymptote, i.e. the backward limit of $\cos(\phi)$ is $-p_x/|p|$. This gives

$$K_+ = p_\phi^2 + f(p_x/|p|) \tag{9}$$

$$K_- = p_\phi^2 + f(-p_x/|p|). \tag{10}$$

We see that K fulfils the asymptotic compatibility condition (2) only if f is an even function. In order to violate (2) we will later take the choice $f(\cos(\phi)) = \cos(\phi) + c$ with $c > 1$ for the numerical computations presented in section 3.

In order to construct the quantum S-matrix for system (7) we start by constructing the eigenfunctions and eigenvalues of K, i.e. we find the solutions of

$$\left[-\hbar^2 \frac{d^2}{d\phi^2} + f(\cos(\phi))\right] \chi_j(\phi) = c_j \chi_j(\phi) \tag{11}$$

with the periodic boundary conditions $\chi_j(\phi + 2\pi) = \chi_j(\phi)$. This is a version of the Mathieu equation. Because H is invariant under the symmetry $\phi \to -\phi$ we obtain an infinite sequence of symmetric solution functions $a_j(\phi)$ with eigenvalues λ_j, $j = 0, 1, \ldots$ and an infinite sequence of anti-symmetric solution functions $b_j(\phi)$ with eigenvalues μ_j, $j = 1, 2, \ldots$. Let the indices be chosen such that λ_j and μ_j are ordered monotonically.

We represent the eigenfunctions a_j and b_j by the coefficients $a_{j,k}$ and $b_{j,k}$ of their decompositions into trigonometric functions according to

$$a_j(\phi) = \sum_{l=0}^{\infty} a_{j,l} gs_l(\phi) \tag{12}$$

where $gs_0(\phi) = (2\pi)^{-1/2}$ and $gs_l(\phi) = \cos(l\phi)\pi^{-1/2}$ for $l \geqslant 1$ and

$$b_j(\phi) = \sum_{l=1}^{\infty} b_{j,l} ga_l(\phi) \tag{13}$$

where $ga_l(\phi) = \sin(l\phi)\pi^{-1/2}$ for $l \geqslant 1$. For $j \to \infty$ we find $\lambda_j \to \hbar^2 j^2$, $a_{j,l} \to \delta_{j,l}$, $\mu_j \to \hbar^2 j^2$, $b_{j,l} \to \delta_{j,l}$. The orthonormality $\sum_{l=0}^{\infty} a_{j,l} a_{k,l} = \delta_{j,k}$, $\sum_{l=1}^{\infty} b_{j,l} b_{k,l} = \delta_{j,k}$ will be useful later in several places. Without loss of generality we choose the free phases of gs and ga such that these functions and also all $a_{j,l}$ and $b_{j,l}$ are real.

Next we need the general solution of the full Schrödinger equation

$$\left[-\frac{\hbar^2}{2r}\frac{\partial}{\partial r} r \frac{\partial}{\partial r} + \frac{1}{2r^2} K - E\right] \psi(r, \phi) = 0. \tag{14}$$

For a symmetrical solution we make the ansatz

$$\psi(r, \phi) = \sum_{j=0}^{\infty} d_j h_j(r) a_j(\phi). \tag{15}$$

For an anti-symmetric solution we make a corresponding ansatz with the angular functions $b_j(\phi)$.

Inserting (15) into (14) gives for h_j the equation

$$\left[-\hbar^2 \frac{1}{2r}\frac{\mathrm{d}}{\mathrm{d}r} r \frac{\mathrm{d}}{\mathrm{d}r} + \frac{\lambda_j}{2r^2} - E\right] h_j(r) = 0 \tag{16}$$

where the regular solution is the Bessel function

$$h_j(r) = J_{\lambda_j^{1/2}/\hbar}((2E)^{1/2} r/\hbar). \tag{17}$$

Inserting this into (15) and performing the asymptotic expansion of the Bessel function for $r \to \infty$ gives the asymptotic form of ψ

$$\psi(r, \phi) \to \sum_{l=0}^{\infty} gs_l(\phi) \sum_{j=0}^{\infty} a_{j,l} d_j \hbar^{1/2} (2\pi r (2E)^{1/2})^{-1/2} [\exp(\mathrm{i}((2E)^{1/2} r/\hbar - \lambda_j^{1/2}\pi/2\hbar - \pi/4)) + \exp(-\mathrm{i}((2E)^{1/2} r/\hbar - \lambda_j^{1/2}\pi/2\hbar - \pi/4))] \tag{18}$$

The incoming wave contribution to angular momentum $l\hbar$, which is given by

$$\hbar^{1/2}(2\pi r(2E)^{1/2})^{-1/2}\exp(-\mathrm{i}((2E)^{1/2}r/\hbar - \pi/4 - l\pi/2))gs_l(\phi)$$

has the coefficient

$$D_l = \sum_{j=0}^{\infty} a_{j,l}d_j \exp(\mathrm{i}(\lambda_j^{1/2}\pi/2\hbar - l\pi/2)). \tag{19}$$

Next we choose for the incoming wave the boundary condition at infinity of only a contribution to angular momentum kh. In order to obtain $D_l = \delta_{l,k}$ we have to make the following choice for d_l:

$$d_l = d_l^{(k)} = a_{l,k}\exp(-\mathrm{i}(\lambda_l^{1/2}\pi/2\hbar - k\pi/2)). \tag{20}$$

Then the coefficient in front of the outgoing wave contribution to angular momentum $l\hbar$, namely

$$\hbar^{1/2}(2\pi r(2E)^{1/2})^{-1/2}\exp(\mathrm{i}((2E)^{1/2}r/\hbar - l\pi/2 - \pi/4))gs_l(\phi)$$

is just the S-matrix element $S_{l,k}^{\mathrm{sym}}$ in the gs representation, i.e.

$$S_{l,k}^{\mathrm{sym}} = \sum_{j=0}^{\infty} a_{j,l}a_{j,k}\exp(-\mathrm{i}(\lambda_j^{1/2}\pi/\hbar - (k+l)\pi/2)). \tag{21}$$

For the anti-symmetric part we obtain along the same lines

$$S_{l,k}^{\mathrm{as}} = \sum_{j=1}^{\infty} b_{j,l}b_{j,k}\exp(-\mathrm{i}(\mu_j^{1/2}\pi/\hbar - (k+l)\pi/2)). \tag{22}$$

At this point we can show in a nice way the significance of the asymptotic compatibility condition (2). If K fulfils (2), i.e. if f is an even function such that $V(r,\phi) = V(r,\phi+\pi)$, then $a_{j,l} = 0$ and $b_{j,l} = 0$ if j, l are not both even or both odd. Then in all contributions in (21) and (22) which are not zero, we find that $j+l$ is even and therefore $\exp(\mathrm{i}(l+j)\pi) = 1$ or

$$\exp(-\mathrm{i}l\pi/2) = \exp(\mathrm{i}j\pi)\exp(\mathrm{i}l\pi/2) \tag{23}$$

and we can cast (21) into the form

$$S_{l,k}^{\mathrm{sym}} = \sum_{j=0}^{\infty} a_{j,l}\exp(\mathrm{i}\pi l/2)\exp(-\mathrm{i}\pi(\lambda_j^{1/2}/\hbar - j))a_{j,k}\exp(-\mathrm{i}\pi k/2). \tag{24}$$

Now S is just a unitary transform of the diagonal matrix $\tilde{S}$ with diagonal elements

$$\tilde{S}_{j,j}^{\mathrm{sym}} = \exp(-\mathrm{i}\pi(\lambda_j^{1/2}/\hbar - j)). \tag{25}$$

In this case the K representation of S, given by (25), is diagonal and the symmetric scattering phases are given by

$$\phi_j = -\pi(\lambda_j^{1/2}/\hbar - j). \tag{26}$$

These eigenphases cross, in general, when some parameter in f is changed such that condition (2) remains valid. An analogue computation holds for the anti-symmetric part of the S-matrix.

If K does not fulfil (2) then (23) is not true for all non-vanishing contributions and accordingly the K representation of S is not diagonal, showing that K is not a conserved quantity of S. In this case the eigenphases of S do not cross under a parameter change of the function f. We learn that the asymptotic compatibility of a second conserved quantity K is necessary in order to make S diagonal in K representation.

3. Eigenphase statistics

Now we make the particular choice of equation (1):

$$f(\cos(\phi)) = c + \cos(\phi) \tag{27}$$

for the potential function f, where $c > 1$ in order to avoid an attractive singularity. Then the conserved quantity

$$K = p_\phi^2 + c + \cos(\phi) \tag{28}$$

of the Hamiltonian does not fulfil (2) and S is not diagonal in the K representation. One might object that besides K there could be another conserved quantity of H which fulfils (2) and which transfers to the S-matrix. This possibility can be ruled out by plots of the classical iterated scattering map M. As labels for the asymptotes we use the direction of the incoming momentum $\alpha = \tan^{-1}(p_y/p_x)$ and the angular momentum p_ϕ. To each set of values of α and p_ϕ there exists exactly one incoming and one outgoing asymptote.

In figure 1 we show how the scattering map changes from near integrable to chaotic as a function of the parameter c. For $c = 4$ we see the onset of chaos along a separatrix as well as numerous stable islands of various periods. For diminishing values of c we see the transition to a large-scale chaotic area. Note that the short-period islands disappear and only long-period islands survive at the edges of the chaotic band. We shall now proceed to a more detailed description of this transition which the reader mainly interested in quantum results may skip.

For c to infinity the $\cos(\phi)$ part of the potential which causes the non-integrability of M is negligible compared to the c part which conserves p_ϕ. Of course, p_ϕ is a conserved quantity of the free motion and it fulfils the asymptotic condition (2). Therefore in the limit of $c \to \infty$ the angular momentum becomes a conserved quantity of H and of M. The lines $p_\phi =$ constant are invariant lines of M and M becomes a pure twist map where the line $p_\phi = 0$ has the winding number 1/2 and the winding number decreases monotonically to 0 on both sides for $|p_\phi| \to \infty$. For c becoming smaller M becomes a perturbed twist map where the quantity $k = (c-1)^{-1}$ is the perturbation parameter. Lines of the pure twist map with rational winding numbers break into finite sequences of alternating stable and unstable periodic points. Around the stable periodic points KAM tori form and along the invariant manifolds of the unstable periodic points small chaotic strips emerge. In total we find the typical scenario of a perturbed twist map as analysed for the standard map [23, 24].

For large c the chaos starts on tiny scales and for decreasing values of c we see numerically appreciable chaos at $c = 4$ for the first time. A numerical plot of the iterated map M for $c = 4$ is presented in figure 1(a). For several initial points (marked by crosses) a few hundred iterates have been plotted. We observe a chaotic strip along the invariant manifolds of the unstable periodic point of period 2. For decreasing c two things happen. The KAM islands first become larger and, at the same time, the chaotic strips along the invariant manifolds of the unstable points also become larger and start to destroy the KAM island from the outside. In particular the chaos eventually destroys such invariant lines with irrational winding numbers, which run around all values of α, thereby forming a large global chaotic sea. Figure 1(b) shows the situation for $c = 3$ where the chaotic strip originating from the unstable periodic point of period 2 has already merged with the chaotic strip belonging to the unstable periodic points of period 3. While the KAM islands are eaten away by the chaotic strips from the outside, at the same time chaos already starts

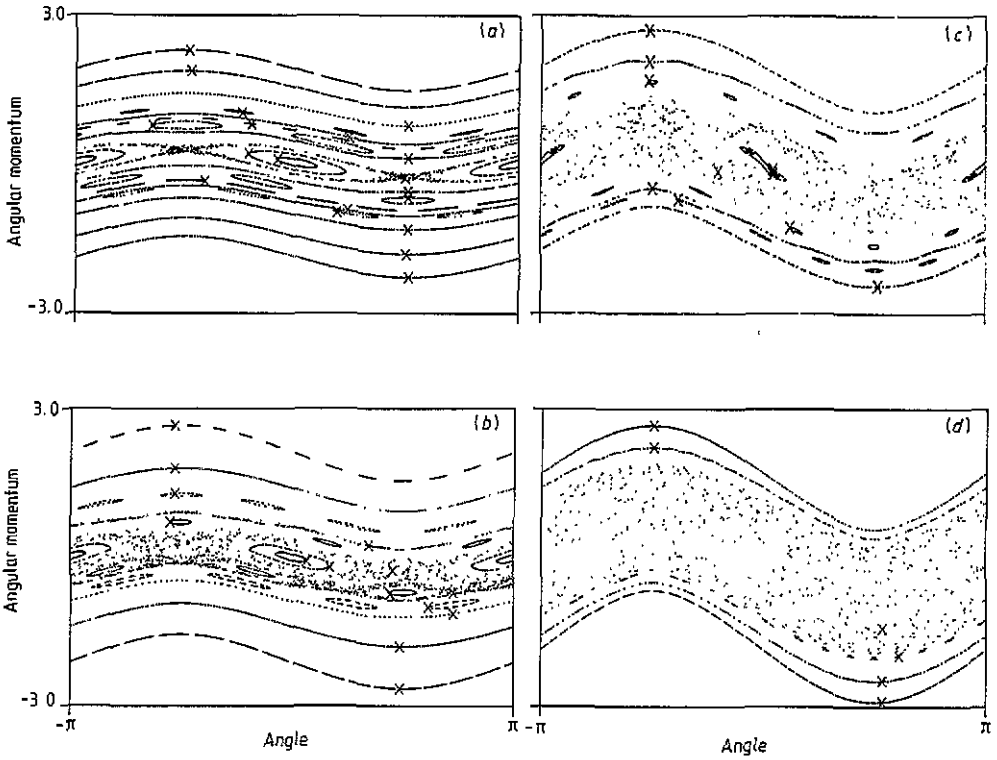

Figure 1. Plot of the classical iterated scattering map for the parameter values $c = 4, 3, 2, 1.2$ in parts (a)–(d) respectively. A few hundred iterates of some initial points (marked by crosses) have been plotted.

to grow in the inside. The central elliptic periodic point of the island becomes unstable in a period-doubling bifurcation creating periodic points of multiple period. In figure 1(c) for $c = 2$ we observe very nicely how the periodic point of period 2 has already become unstable and has created a periodic point of period 4 close to it. All this happens behind a KAM line which screens this event from the large chaotic sea. For $c = 2$ the large chaotic sea has already reached the region of winding number 1/5. For c a little bit below 2 all large scale KAM islands at small values of p_ϕ are destroyed. A typical plot of M for this behaviour is given in figure 1(d) for $c = 1.2$. There still exist very small KAM islands inside the large chaotic sea. They are not relevant for our further considerations. The chaotic sea also does not spread to arbitrarily large values of p_ϕ. As figure 1(d) demonstrates it stops approximately at winding number 1/6. For larger values of p_ϕ order always dominates even though there are very tiny chaotic strips associated with every rational winding number arbitrarily far outside. However, these tiny chaotic strips are also not relevant for our further considerations.

Next let us turn to the numerical properties of the quantum S-matrix which is the quantization of the map M. Of course, in the S-matrix in the angular momentum representation indications of chaos can also be expected in a finite block only, which corresponds to the finite chaotic strip in the plot of the classical scattering map. In the classical plot in figure 1(d) the strip strongly dominated by chaos reaches from $p_\phi = -1.2$

to $p_\phi = 1.2$ approximately. Therefore we expect in the symmetric as well as in the anti-symmetric S-matrix a block of size

$$N = 1.2/\hbar \tag{29}$$

to be dominated by chaos for small values of c. Beyond this block the S-matrix makes a transition to regular behaviour and for $j^2\hbar^2 \gg c$ the S-matrix approaches a diagonal form with scattering phases

$$\phi_j \to -\pi c/(2j\hbar^2). \tag{30}$$

This asymptotic form holds for the symmetric as well as for the anti-symmetric part of the S-matrix.

We wish to have reliable results for the eigenstates corresponding to the chaotic area which is largest for the smallest value $c = 1.5$ which we use in quantum calculations. Using $\hbar = 0.001\,25$ this area corresponds to about 1000 to 1200 states for both the symmetric and the anti-symmetric case separately. In order to obtain these states reliably we diagonalize matrices of the size 3200×3200 on the CRAY YMP of Universidad National Autonoma de Mexico.

To select the relevant block in this large S-matrix we can do something even better. We construct S in the K representation and select the block of size $N \times N$ with N given by (29). The K representation corresponds to a classical picture where the $\cos(\alpha)$ wave in figure 1 has been straightened out. Therefore in the K representation the cut-off between chaos and order is best given by a horizontal line.

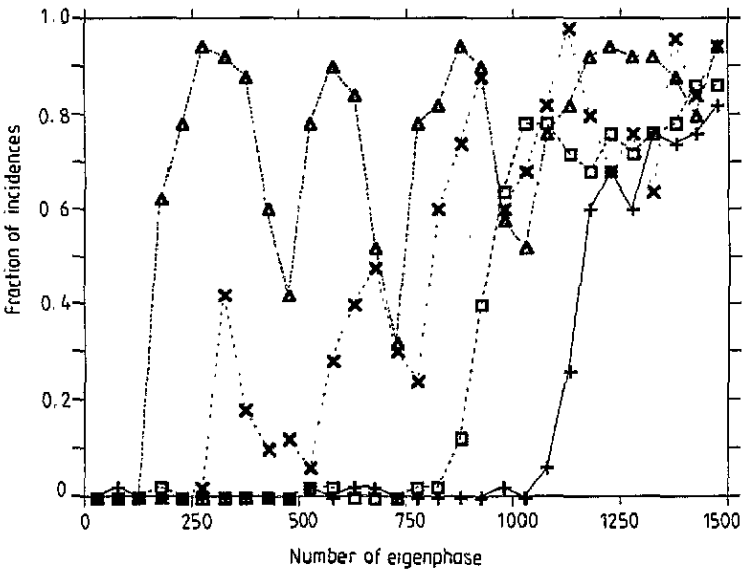

Figure 2. Relative fraction of incidences between symmetric and anti-symmetric eigenphases of the S-matrix. Each data point shows the result of a block of eigenphases of length 50. The vertical crosses, open squares, inclined crosses and open triangles correspond to $c = 5, 3, 2, 1.5$ respectively. $\hbar = 0.001\,25$.

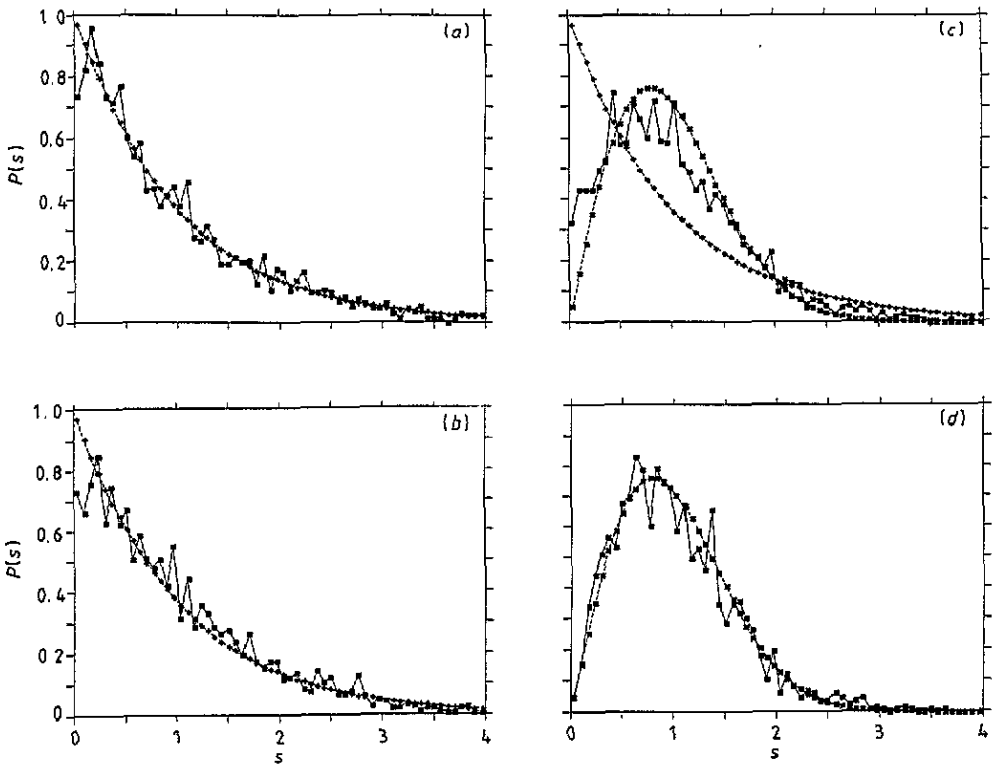

Figure 3. Nearest-neighbour spacing distributions of the eigenphases for the parameter values $\hbar = 0.001\,25$ and $c = 5, 3, 2, 1.5$ in parts (a)–(d) respectively (full squares). From the symmetric and anti-symmetric S-matrix a block of size $N = 1000$ has been evaluated. The symmetric and anti-symmetric results have been averaged. Parts (a), (b) and (c) also contain the theoretical prediction for a random sequence (vertical crosses). Parts (c) and (d) also contain the theoretical prediction of COE (inclined crosses).

The choice of (29) has been justified by semiclassical arguments. There is a different justification completely within quantum dynamics. We compute the eigenphases ϕ_j^{sym}, $j = 0, 1, \ldots$ of the symmetric S-matrix and the eigenphases ϕ_j^{as}, $j = 1, 2, \ldots$ of the anti-symmetric S-matrix and check the coincidence of ϕ_j^{sym} with ϕ_j^{as}. In the chaotic region there is no correlation between them whereas in the regular region we find $|\phi_j^{\text{sym}} - \phi_j^{\text{as}}| < 10^{-4}$ for a large fraction of all eigenphases even though j is still far away from values where (30) holds. In figure 2 we plot the fraction of symmetric and anti-symmetric pairs of eigenphases that are within these limits as a function of the number of states counted from the centre of the band and evaluated over blocks of 50 states. The four curves shown corresponds to values $c = 5, 3, 2, 1.5$. We note that the cut-off is clear for $c = 1.5$ and 2, while we obtain oscillating curves for the larger values of c. This is readily understood as in this parameter region integrable islands occupy most of the phase space. The numerical results in what follows are given for a choice of $N = 1000$ for the cut-off which we keep fixed when we vary c.

In figure 3 we present the distribution of the nearest-neighbour spacings of the eigenvalues of the S-matrix for the values $c = 5, 3, 2, 1.5$ of the potential constant in parts

(a)–(d) respectively. The results of the symmetric and the anti-symmetric S-matrix have been averaged because of their statistical independence. For comparison the corresponding curves for a COE and for a Poisson distribution have been included in some of the figures.

For $c = 1.5$ in figure 3(d), where the classical map is dominated by chaos, the quantum result is very close to the COE behaviour. For $c = 2$ in figure 3(c) we see small deviations from the COE behaviour in parallel to the appearance of the first KAM tori around $p_\phi = 0$ in the classical plot of figure 1(c). For $c = 3$ where classically the transition to global order takes place the quantum result is just in a transition to Poisson behaviour. For $c = 5$ in figure 3(a) where the classical chaos has diminished to invisible size, the quantum result is very close to the Poisson distribution which we expect for a completely integrable S-matrix. Only for very small distances do we see that the S-matrix is not completely integrable.

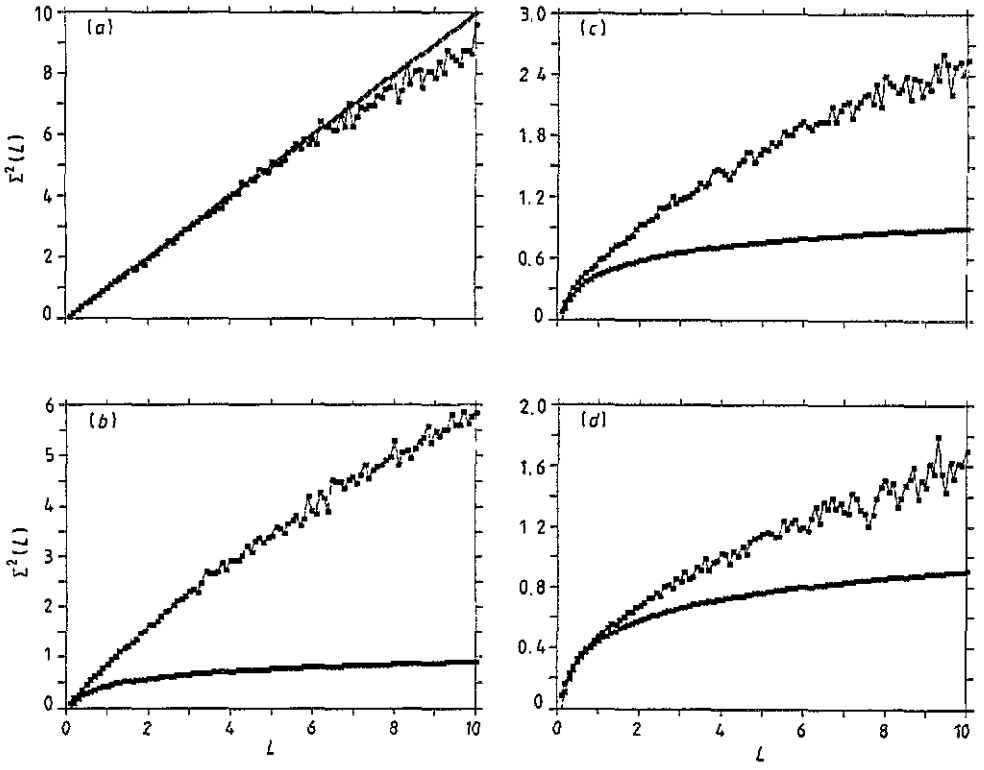

Figure 4. Σ^2 statistics of the eigenphases for the parameter values $\hbar = 0.001\,25$ and $c = 5, 3, 2, 1.5$ in parts (a)–(d) respectively (full squares). From the symmetric and anti-symmetric S-matrix a block of size $N = 1000$ has been evaluated. The symmetric and anti-symmetric results have been averaged. Part (a) also contains the theoretical prediction for a random sequence (vertical crosses). Parts (b), (c) and (d) also contain the theoretical prediction of COE (inclined crosses).

In figure 4 we present the corresponding Σ^2 statistics for the same parameter values. Again the symmetric and anti-symmetric results have been averaged. For increasing values of c there is a transition from behaviour close to COE to a behaviour close to Poisson. This holds for small values of the distance L. For $c = 1.5$ in figure 4(d) the function rises linearly with a slope 1 over a very short distance only (interval from 0 to 0.3) whereas for $c = 5$ in figure 4(a) this linear increase with slope 1 is maintained until $L = 7$ approximately. In addition for $c = 1.5$ the numerical result is always a little larger than the COE prediction

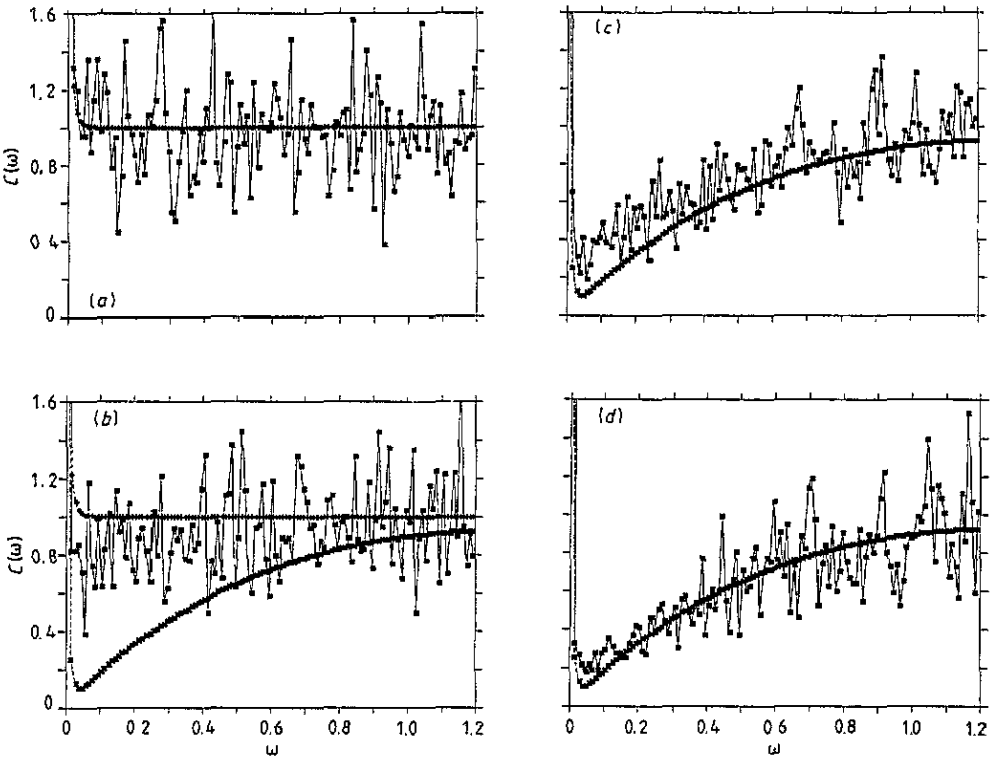

Figure 5. Fourier transform of the spectrum of the S-matrix for the parameter values $\hbar = 0.00125$ and $c = 5, 3, 2, 1.5$ in parts (a)–(d) respectively (full squares). From the symmetric and anti-symmetric S-matrix a block of size $N = 1000$ has been evaluated. The symmetric and anti-symmetric results have been averaged. Parts (a) and (b) also contain the theoretical prediction for a random sequence (vertical crosses). Parts (b), (c) and (d) also contain the theoretical prediction of COE (inclined crosses).

and deviates significantly for $L > 1.5$. So we suppose that the S-matrix always has less long-range correlations in the spectrum than we expect for the COE.

In order to obtain a better understanding of these long-range fluctuations we consider in figure 5 the Fourier transform of the spectrum of eigenphases, i.e. the function

$$C^{\mathrm{sym/as}}(\omega) = \sum_j \exp\left(i\omega\phi_j^{\mathrm{sym/as}}\right). \tag{31}$$

Again the symmetric and anti-symmetric results have been averaged. On small frequency scales (order of $\omega \approx 0.001$) the function C oscillates wildly. Therefore in the figure we have averaged this function over a length of $\omega = 0.01$, however $C(\omega)$ still shows strong fluctuations. For $c = 1.5$ there is a very clear correlation hole at small values of ω. The average of the numerical result comes close to the COE prediction:

$$C^{\mathrm{COE}}(\omega) = 2\omega - \omega\ln(1+2\omega) + (2\pi^2\omega^2 N)^{-1} \tag{32}$$

also plotted in the figure. The last term in (32) results from the finite cut-off at N [25]. The correlation hole in the numerical result (figure 5(d)) is not quite as deep as the one in the

theoretical curve according to (32). We find that this deviation occurs at frequencies below 0.2 for $c = 1.5$.

For $c = 2$ in figure 5(c) the correlation hole is less deep than for $c = 1.5$ and accordingly the deviation from (32) has become larger. For $c = 3$ in figure 5(b) the hole has been filled up to a level 0.8 on the average and for $c = 5$ in figure 5(a) the average behaviour is very close to the one of an integrable case where we expect

$$C^{\text{int}}(\omega) = 1 + (2\pi^2\omega^2 N)^{-1}.$$

4. Conclusions

We have studied a particularly simple scattering system with the following properties:

(i) the Hamiltonian is integrable and, as a consequence, no topological chaos exists;

(ii) the classical scattering map is non-integrable and for certain values of a parameter clearly displays a chaotic region in the channel space. In this region only very small elliptic islands appear which furthermore have large periods.

The corresponding quantum mechanical problem may be solved in closed form in the sense that the S-matrix elements can be given in terms of Fourier coefficients of well known special functions. On the other hand if we restrict the S-matrix to channels associated with the chaotic region in the channel space we find fair agreement with the COE, which is one of the classical ensembles and characteristic of chaos in time-reversal invariant systems. This explicitly confirms the result found on general grounds in [14–16].

A significant deviation is found in the long-range part of the two-point function as seen both in Σ^2 and the low-frequency range of the Fourier transform. Whether this deviation is due to some general properties or is a property of the particular map we chose is at this moment not clear. Note though that we find an excess in fluctuations rather than in long-range stiffness and this might simply be due to the remaining islands.

We may now ask whether the situation of a chaotic scattering map associated with an integrable Hamiltonian is very particular or rather general. This depends, as mentioned above, on the interplay of the complete Hamiltonian and the free Hamiltonian. If the constants of motion responsible for the integrability of the full Hamiltonian are also constants of motion for the free Hamiltonian then integrability is readily transferred from the Hamiltonian to the scattering map. For example this happens for all rotationally invariant systems. Yet we have seen that such a condition—while sufficient—is not necessary, for the integrability of the Hamiltonian to entail that of the scattering map. A nice example is the Hamiltonian (7) if we choose $f(\phi) = \cos(2\phi) + c$. In fact almost any small change in the Hamiltonian (that does not conserve the symmetry) will lead to a non-integrable scattering map even if it leaves the Hamiltonian integrable. We may give a more mathematical formulation of this scenario as follows.

It is appropriate to order scattering systems into three classes with respect to their integrability properties:

Class 1: M and also H are completely integrable;

Class 2: M is not integrable, but H is integrable; and

Class 3: neither M nor H is integrable.

Class 2 is not a rare exception because the absence of periodic orbits is structurally stable and this, in turn, implies the stability of the absence of invariant sets. This is true except for some pathological behaviour at energy $E = 0$. Note though that the complete

integrability of M is not structurally stable. Moreover, there are many scattering systems having topological scattering chaos for a finite interval of positive energy values only. For larger values of E there is no longer topological chaos on the energy shell, whereas the iterated scattering map is still chaotic.

Under these circumstances we will have to consider carefully which properties of a quantum scattering system are signatures of chaos in the scattering map or of topological chaos respectively. Clearly eigenphase statistics are associated with the first and time delays with the second property of the classical system. The latter is seen trivially as time delays are associated with the energy derivative of the eigenphases which are energy independent in our example. Other properties, more accessible to most experiments, will have to be examined carefully, which we plan to do in a forthcoming paper.

Acknowledgments

One of the authors (CJ) thanks the Deutsche Forschungsgemeinschaft for a Heisenberg stipendium. This work was supported by the University of Mexico DGAPA contract IN-100491 and by the contract SC-101094 of CRAY Research and the University of Mexico.

References

[1] Mehta M L 1991 *Random Matrices and the Statistical Theory of Energy Levels* (New York: Academic)
[2] Bohigas O, Giannoni M J and Schmit C 1984 *Phys. Rev. Lett.* **52** 1
[3] Wintgen D and Friedrich H 1986 *Phys. Rev. Lett.* **57** 571
[4] Delande D and Gay J C 1986 *Phys. Rev. Lett.* **57** 2006
[5] Holle A, Main J, Weisbuch G, Rottke H and Welge K H 1988 *Phys. Rev. Lett.* **61** 161
[6] Seligman T H, Verbaarschot J J M and Zirnbauer M 1984 *Phys. Rev. Lett.* **53** 215; 1985 *J. Phys. A: Math. Gen.* **18** 2751
[7] Bohigas O, Tomsovic S and Ullmo D 1990 *Phys. Rev. Lett.* **64** 1479; **65** 5
[8] Lombardi M, Pique J P, Labastie P, Broyer M and Seligman T H 1991 *Comments At. Mol. Phys.* **25** 345
[9] Pique J P, Chen Y, Field R W and Kinsey J L 1987 *Phys. Rev. Lett.* **58** 3479
[10] José J V and Cordery R 1986 *Phys. Rev. Lett.* **56** 290
[11] Izrailev F M 1990 *Phys. Rep.* **196** 299
[12] Smilansky U 1992 *Proc. 1989 Les Houches Summer School* ed M J Giannoni, A Voros and J Zinn-Justin (Amsterdam: North-Holland) pp 371–441
[13] Berry M V 1985 *Proc. R. Soc.* A **400** 229
[14] Blümel R and Smilansky U 1990 *Phys. Rev. Lett.* **64** 241
[15] Leyvraz F and Seligman T H 1992 *Phys. Lett.* **168A** 348
[16] Seligman T H 1994 *Quantum Chaos* ed G Casati and B Chirikov (Cambridge: Cambridge University Press) (at press)
[17] Jung C 1993 *J. Phys. A: Math. Gen.* **26** 1091
[18] Jung C 1993 *Ann. Phys.* **228** 158
[19] Blümel R, Dietz B, Jung C and Smilansky U 1992 *J. Phys. A: Math. Gen.* **25** 1483
[20] Jung C 1986 *J. Phys. A: Math. Gen.* **19** 1345
[21] Jung C 1987 *J. Phys. A: Math. Gen.* **20** 1719
[22] Jung C 1991 *J. Phys. A: Math. Gen.* **24** 1741
[23] Chirikov B V 1979 *Phys. Rep.* **52** 263
[24] Greene J M 1979 *J. Math. Phys.* **20** 1183
[25] Lombardi M and Seligman T H 1993 *Phys. Rev.* A **47** 3571